A universal variable extension method for designing multi-scroll/wing chaotic systems

Hairong Lin, *Member, IEEE*, Chunhua Wang, and Yichuang Sun, *Senior Member, IEEE*

Abstract—Developing a universal design method to construct different multi-scroll/wing chaotic systems (MS/WCSs) has been challenging. This paper proposes a general design method for MS/WCSs called the universal variable extension method (UVEM). It is a simple but effective approach that generates 1-direction (1-D) and 2-D multi-scroll/wing chaotic attractors. Using any double-scroll/wing chaotic system as the basic system, the UVEM is able to construct different MS/WCSs. Employing Chua's chaotic system and Lorenz chaotic system as two examples, we construct two MSCSs (including 1-D and 2-D) and two MWCSs (including 1-D and 2-D), respectively. Theoretical analysis and numerical simulation show that the constructed MS/WCSs not only can generate 1-D and 2-D multi-scroll/wing chaotic attractors but also have 1-D and 2-D initial boosting behaviors. This means that the MS/WCSs designed by the UVEM are very sensitive to their initial states, and have better unpredictability and more complex chaotic behaviors. To show the simplicity of UVEM in hardware implementation, we develop a field-programmable gate array (FPGA)-based digital hardware platform to implement the designed MS/WCSs. Finally, a new pseudo-random number generator is proposed to investigate the application of the MS/WCSs. All P-values obtained by the NIST SP800-22 test are larger than 0.01, which indicates that the MS/WCSs designed by UVEM have high randomness.

Index Terms—Chaotic system, multi-scroll/wing chaotic attractors, initial boosting behavior, FPGA implementation, PRNG.

I. INTRODUCTION

AS chaotic systems are widely used in nonlinear system control, secure communication, and many other applications, designing chaotic systems with complex dynamics has gained significant attention in recent decades [1, 2]. Among the research works, the design of multi-scroll/wing chaotic systems (MS/WCSs) with high complexity and adjustability has attracted particular interests [3]. Numerous researchers have devoted to their system modeling and dynamic characteristics [4, 5]. A lot of design methods of the MS/WCSs have been proposed [6, 7], however they still encounter some drawbacks and challenges. A dominant problem is that there is no universal method to construct MSCSs and MWCSs. This problem restricts the flexibility of the generation of multi-scroll/wing chaotic attractors (MS/WCAs) and makes MS/WCS application difficult. Therefore, finding a novel design method that can be applied to construct both MSCSs and MWCSs is still challenging and significant work.

Over the past decades, much research has been published on the design methods of MS/WCSs. As the pioneering research, Suykens and Vandewalle [8] constructed the first MSCS by using a quasilinear approach in 1991. Since then, the construction of MS/WCSs has attracted many researchers'. Particularly, Yu *et al*. [9] put forward many key theories on the construction of MS/WCSs, and successively proposed a series of control methods

of nonlinear functions including stair function [10], sawtooth wave function [11], piecewise-linear function [12], switching function [13]. The basic theory is that the MS/WCAs can be generated by using the nonlinear functions to increase the number of unstable saddle focus equilibrium points in double-scroll/wing chaotic systems (DS/WCSs). In the last ten years, according to this basic theory, various nonlinear functions have been applied to design MS/WCSs based on different DS/WCSs such as Lorenz-like systems [14, 15], Chua-like systems [16, 17], Sprott-like systems [18, 19], Jerk-like systems [20, 21], and so on [22, 23]. In recent years, with the development of the research, some MS/WCSs have been proposed by adopting non-function control methods. For example, Hong *et al*. [24, 25] constructed a series of MWCSs by using multilevel pulses to replace the original variables of the basic double-wing chaotic systems. Wang *et al*. [26] realized an MSCS by using a piecewise-linear Chua's diode to replace the nonlinear resistor of the Chua's circuit. Zhang *et al*. [3, 27] proposed an MSCS and an MWCS by coupling a multi-piecewise linear memristor into a Jerk system and a Sprott system, respectively. Moreover, some other approaches like symmetry conversion [28], fractal transformation [29], and neural networks [30, 31] have also been reported.

The above review shows that to obtain different MS/WCSs a large number of design methods have been developed. However, no matter which method is used, there exist three serious drawbacks: (i) Different design methods are needed for designing different MSCSs and MWCSs, and a universal method is not available. (ii) Different nonlinear functions are required to construct different MS/WCSs, and there is no unified control function. (iii) The realization process is complex, as the basic DS/WCSs must be changed. Clearly, the implementation of different MS/WCSs is very complex and difficult. For a class of practical dynamic systems, a unified nonlinear control is significant [32, 33]. Consequently, a universal method is attractive to design different MS/WCSs, but it is a challenging task, as the basic double-scroll/wing systems and control functions are not universal.

To solve the above issues, this paper proposes a simple universal variable extension method (UVEM). The UVEM has four advantages: (a) By using UVEM, not only the MSCSs can be constructed based on any double-scroll chaotic systems but also the MWCSs can be constructed based on any double-wing chaotic systems; (b) It only needs to adopt the same steps and the same control functions no matter whether to design MSCSs or MWCSs; (c) Design of both 1-D MS/WCSs and 2-D MS/WCSs has the same methods and the same control functions; (d) The UVEM does not change basic DS/WCSs. Undoubtedly, the constructed MS/WCSs by using UVEM have very simple algorithms, system models, and circuits. Therefore, the design, implementation and maintenance of the MS/WCSs have a lower cost. For different requirements, the double-scroll/wing systems can be flexibly replaced. Besides, due to their versatility, they have a wider range of applications in practical engineering scenarios including computers, digital signatures, communication, and information encryption. The main contributions of this paper are summarized as follows.

1) An universal variable extension method is proposed to design different multi-scroll/wing chaotic systems.

2) Based on the UVEM, two MSCSs (1-D and 2-D) and two MWCSs (1-D and 2-D) are designed, and their chaos mechanism, as well as dynamics characteristics, are revealed.

3) An FPGA-based experiment platform is developed to implement the designed MS/WCSs in hardware devices.

The rest of this paper is arranged as follows. Section II introduces the UVEM and discusses its characteristics. Section III provides two examples of MSCSs designed by UVEM. Section IV provides two examples of MWCSs designed by UVEM. Section V implements them in the hardware platform. Section VI presents a comparison and application in PRNGs. Section VII concludes this paper.

II. UNIVERSAL VARIABLE EXTENSION METHOD

In this section, the design flow of the UVEM is proposed firstly. Then, its characteristics are analyzed theoretically.

A. Design Flow

Generally speaking, the construction of MS/WCSs must be based on basic DS/WCSs and nonlinear control functions. The standard model of the 3-dimensional basic DS/WCS can be expressed as

$$\begin{cases} \dot{x} = f_1(x,y,z) \\ \dot{y} = f_2(x,y,z) \\ \dot{z} = f_3(x,y,z) \end{cases} \tag{1}$$

Where x, y, and z are three state variables. f_1, f_2, and f_3 are three corresponding state equations. Here, we introduce a unified nonlinear multi-piecewise-linear function as follows

$$F(\varphi) = \begin{cases} \varphi, N = 0 \\ \varphi - \sum_{i=1}^{N}(\text{sgn}(\varphi + (2i-1)) + \text{sgn}(\varphi - (2i-1))), N = 1,2,3,\ldots \\ \varphi - \text{sgn}(\varphi), M = 0 \\ \varphi - \text{sgn}(\varphi) - \sum_{j=1}^{M}(\text{sgn}(\varphi + 2j) + \text{sgn}(\varphi - 2j)), M = 1,2,3,\ldots \end{cases} \tag{2}$$

where sgn(.) is a sign function. As we can see, $F(\varphi)$ can be adjusted by selecting integer control parameters N and M. To visually understand $F(\varphi)$, Fig.1 gives the corresponding curves of $F(\varphi)$ with $N=0$, $M=0$, $N=1$, and $M=1$, respectively. From Fig.1, with the increase of control parameters, the function curves can be extended along two opposite directions at the φ-axis. That is to say, the proposed $F(\varphi)$ has an extension function. Especially, the odd (blue points) or even (red points) number of the points of intersection with the φ-axis can be obtained with the increase of control parameters N and M. That is to say, any number of extension multiples can be realized by adjusting N and M, as shown in Table I, thus generating odd numbers and even numbers of scrolls/wings by selecting different values of N or M.
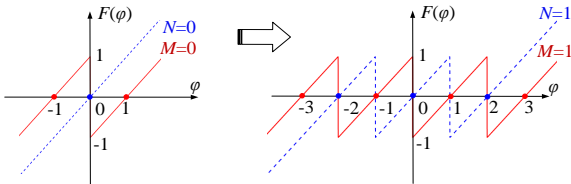

Fig. 1: Curves of control function $F(\varphi)$ with $N=0$, $M=0$, $N=1$, and $M=1$.

TABLE I: EXTENSION MULTIPLES DEPENDENT ON CONTROL PARAMETERS.

N	Extension multiples	M	Extension multiples
0	1	0	2
1	3	1	4
2	5	2	6
…	…	…	…
N	$2N+1$	M	$2M+2$

Next, a UVEM to design 1-D and 2-D MS/WCSs is proposed based on the basic system (1). Most of the existing design methods of MS/WCSs must modify the basic systems by using different nonlinear control functions to replace or couple original variables. As a result, its electronic circuit realization is complicated due to the use of multiple control functions. Also, both the basic systems and variables are destroyed, which is not conducive to its implementation. Therefore, a simple UVEM without changing basic systems is presented. The realization process has only one step for constructing 1-D MS/WCSs. By extending one state variable φ and adding one extended state equation $\dot{\varphi}=cx+dF(\varphi)$ to the basic system (1), a 1-D MS/WCS can be constructed as follows

$$\begin{cases} \dot{x} = f_1(x,y,z) \\ \dot{y} = f_2(x,y,z) \\ \dot{z} = f_3(x,y,z) \\ \dot{\varphi} = cx - dF(\varphi) \end{cases} \tag{3}$$

where φ is the extension variable, $F(\varphi)$ is the nonlinear control function, and c and d are defined as non-zero relevant parameters and extension coefficients, respectively. Similarly, by extending two state variables φ_1 and φ_2 and adding two extended state equations $\dot{\varphi}_1=c_1x+d_1F_1(\varphi_1)$ and $\dot{\varphi}_2=c_2x+d_2F_2(\varphi_2)$ to the basic system (1), a 2-D MS/WCS can be constructed as follows

$$\begin{cases} \dot{x} = f_1(x,y,z) \\ \dot{y} = f_2(x,y,z) \\ \dot{z} = f_3(x,y,z) \\ \dot{\varphi}_1 = c_1x - d_1F_1(\varphi_1) \\ \dot{\varphi}_2 = c_2y - d_2F_2(\varphi_2) \end{cases} \tag{4}$$

where φ_1 and φ_2 are two extension variables, and F_1 and F_2 are nonlinear control functions. c_1, c_2, d_1, and d_2 are defined as non-zero relevant parameters and extension coefficients, respectively. It can be seen from systems (3) and (4) that the basic system (1) has not been changed, and only extended state equations are needed. There is no doubt that the implementation process of the UVEM is very simple. In addition, this method only needs a unified nonlinear control function, which largely simplifies the system model, algorithm, and circuit of the MS/WCSs.

Moreover, to better understand and apply this design method, a design flow graph based on the proposed UVEM is given in Fig.2. From Fig.2, the UVEM can be easily realized by expanding new state variables. 1-D MS/WCAs can be generated by expending one new variable, and 2-D MS/WCAs can be obtained by expending two new variables. More importantly, the two steps only require the same control function. Therefore, the UVEM only requires one step to realize 1-D MS/WCSs and two steps to realize 2-D MS/WCSs. Also, no matter whether MSCSs or MWCSs, only the same steps and the same nonlinear control function are needed.
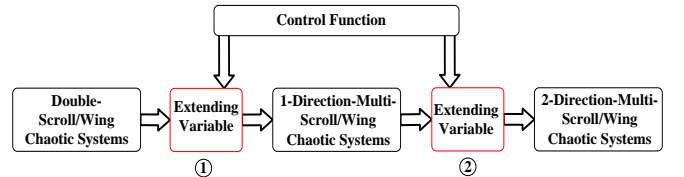

Fig. 2: Design flow graph of the UVEM.

B. Theoretical Analysis

In this subsection, the symmetry, divergence, and stability of the 1-D and 2-D MS/WCSs designed by UVEM are studied. According to equation (2), there is $F(\varphi)=-F(\varphi)$. Therefore, from systems (3) and (4), we can have the following inference:

Inference 1: The 1-D MS/WCS in system (3) is of inversion symmetry about φ. The 2-D MS/WCS in system (4) is of inversion symmetry about φ_1 and φ_2.

The super volume shrinkage rate of systems (3) and (4) can be calculated by

$$\nabla V_1 = \frac{\partial \dot{x}}{\partial x} + \frac{\partial \dot{y}}{\partial y} + \frac{\partial \dot{z}}{\partial z} + \frac{\partial \dot{\varphi}}{\partial \varphi} = \left(\frac{\partial \dot{x}}{\partial x} + \frac{\partial \dot{y}}{\partial y} + \frac{\partial \dot{z}}{\partial z} \right) - d = \varepsilon - d \quad (5)$$

$$\nabla V_2 = \frac{\partial \dot{x}}{\partial x} + \frac{\partial \dot{y}}{\partial y} + \frac{\partial \dot{z}}{\partial z} + \frac{\partial \dot{\varphi}_1}{\partial \varphi_1} + \frac{\partial \dot{\varphi}_2}{\partial \varphi_2} = \left(\frac{\partial \dot{x}}{\partial x} + \frac{\partial \dot{y}}{\partial y} + \frac{\partial \dot{z}}{\partial z} \right) - d_1 - d_2$$
$$= \varepsilon - (d_1 + d_2) \quad (6)$$

where ε denotes the super volume shrinkage rate of the original double-scroll/wing chaotic systems. Since ε is always less than 0, the shrinkage rate depends on the evolution of extension coefficients d, d_1, and d_2. Therefore, we can get the following inference:

Inference 2: When $d > 0$, $\nabla V_1 = \varepsilon - d < 0$, system (3) is dissipative. 1-D MS/WCS satisfies the necessary conditions for generating chaos. When $d_1 + d_2 > 0$, $\nabla V_2 = \varepsilon - (d_1 + d_2) < 0$, system (4) is dissipative. 2-D MS/WCS satisfies the necessary conditions for generating chaos.

The stability of the 1-D and 2-D MS/WCSs is investigated by analyzing the equilibrium points of systems (3) and (4). Firstly, letting $\dot{x} = \dot{y} = \dot{z} = \dot{\varphi} = 0$, the equilibrium equation of the system (3) can be described as

$$\begin{cases} f_1(x,y,z) = 0 \\ f_2(x,y,z) = 0 \\ f_3(x,y,z) = 0 \\ cx - dF(\varphi) = 0 \end{cases} \quad (7)$$

Solving equation (7), the equilibrium points of system (3) can be obtained by

$$E(x,y,z,\varphi) = (x*, y*, z*, F(\varphi) = cx*/d) \quad (8)$$

where $x*$, $y*$, and $z*$ are the equilibrium points of the original double-scroll/wing chaotic systems. Obviously, the equilibrium point on the φ phase depends on the parameters c, d, and the original equilibrium point $x*$. Combined with the features of $F(\varphi)$, it can be found that the equilibrium points of the system in the x direction are extended along the φ direction. The Jacobian matrix of system (3) can be calculated by

$$J = \begin{bmatrix} \frac{\partial \dot{x}}{\partial x} & \frac{\partial \dot{x}}{\partial y} & \frac{\partial \dot{x}}{\partial z} & \frac{\partial \dot{x}}{\partial \varphi} \\ \frac{\partial \dot{y}}{\partial x} & \frac{\partial \dot{y}}{\partial y} & \frac{\partial \dot{y}}{\partial z} & \frac{\partial \dot{y}}{\partial \varphi} \\ \frac{\partial \dot{z}}{\partial x} & \frac{\partial \dot{z}}{\partial y} & \frac{\partial \dot{z}}{\partial z} & \frac{\partial \dot{z}}{\partial \varphi} \\ \frac{\partial \dot{\varphi}}{\partial x} & \frac{\partial \dot{\varphi}}{\partial y} & \frac{\partial \dot{\varphi}}{\partial z} & \frac{\partial \dot{\varphi}}{\partial \varphi} \end{bmatrix} = \begin{bmatrix} \frac{\partial \dot{x}}{\partial x} & \frac{\partial \dot{x}}{\partial y} & \frac{\partial \dot{x}}{\partial z} & 0 \\ \frac{\partial \dot{y}}{\partial x} & \frac{\partial \dot{y}}{\partial y} & \frac{\partial \dot{y}}{\partial z} & 0 \\ \frac{\partial \dot{z}}{\partial x} & \frac{\partial \dot{z}}{\partial y} & \frac{\partial \dot{z}}{\partial z} & 0 \\ c & 0 & 0 & -d \end{bmatrix} \quad (9)$$

For the equilibrium points E, the characteristic equation can be written by

$$P_1(\lambda) = det|\lambda I - J| = (\lambda + d)P_o(\lambda) \quad (10)$$

where $P_o(\lambda)$ is the characteristic equation of the original double-scroll/wing chaotic systems. Obviously, when $d > 0$, there is an additional characteristic value $\lambda_4 = -d < 0$. Thus the stability of the 1-D MS/WCSs can be derived as follows:

Inference 3: If $d > 0$, the 1-D MS/WCS has the same stability as the original double-scroll/wing chaotic systems, otherwise it is unstable.

By using a similar method, the characteristic equation of system (4) can be deduced as

$$P_2(\lambda) = (\lambda + d_1)(\lambda + d_2)P_o(\lambda) \quad (11)$$

When both $d_1 > 0$ and $d_2 > 0$, there are two additional characteristic values $\lambda_4 = -d_1 < 0$ and $\lambda_5 = -d_2 < 0$. Thus, the stability of the 2-D MS/WCSs can be stated as below:

Inference 4: If $d_1 > 0$ and $d_2 > 0$, the 2-D MS/WCS has the same stability as the original double-scroll/wing chaotic systems, otherwise it is unstable.

Next, two examples using UVEM are given based on double-scroll Chua's system and double-wing Lorenz system, respectively.

III. MSCSs BASED ON CHUA'S SYSTEM

This section designs Chua's system-based 1-D and 2-D MSCSs using UVEM, discusses their chaos mechanisms, and analyzes their dynamical behaviors.

A. Brief Introduction of Chua's system

The classical model of Chua's chaotic system can be expressed as [34]

$$\begin{cases} \dot{x} = a(y-f) \\ \dot{y} = x - y + z \\ \dot{z} = by \end{cases} \quad (12)$$

where f is the piecewise-linear function $m_1 x + 0.5(m_0 - m_1)(|x+1| - |x-1|)$. When parameters $a=9$, $b=-14.286$, $m_0=-1/7$, $m_1=2/7$, and initial states (0.1, 0.1, 0.1), the equilibrium points (red) and attractors (blue) of the system (12) are given in Fig.3. Clearly, the Chua's system generates a standard double-scroll chaotic attractor with one index-1 saddle-focus (P_2) and two index-2 saddle-focus (P_1 and P_3). The mapping results on $x-y$ phase plane and $x-z$ phase plane are plotted in Fig.3(a) and Fig.3(b), respectively.
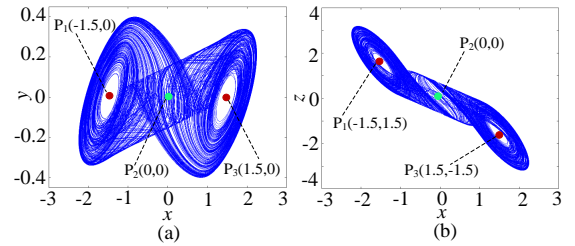
Fig. 3: Double-scroll attractor of system (1). (a) x-y plane. (b) x-z plane.

B. Designing 1-D MSCS Via Extending One State Variable

According to the proposed UVEM, a 1-D MSCS based on Chua's system (12) can be constructed as follows

$$\begin{cases} \dot{x} = a(y-f) \\ \dot{y} = x - y + z \\ \dot{z} = by \\ \dot{\varphi} = cx - dF(\varphi) \end{cases} \quad (13)$$

where c and d are relevant parameters and extension coefficients, respectively. Firstly, the dynamical behavior related to the two parameters (c and d) is investigated by using bifurcation diagrams and Lyapunov exponents. We set one of the parameters c, d, to a fixed value and use the other as a variable to investigate the dynamical behaviors of the 1-D MSCS. Taking $M=1$ as an example, Fig.4 shows two bifurcation plots and the corresponding Lyapunov exponents. As illustrated in Fig.4(a), when fixing $d=21.8$ and increasing c in the region (8, 14), the 1-D MSCS shows the chaos bifurcation scenario within the whole parameter interval. Surprisingly, as the parameter c increases, the motion trajectory starts from chaos with one double-scroll structure ($s_1 \in (8, 9.8)$), goes into chaos with four double-scroll structures ($s_2 \in (9.8, 10.4)$), and finally settles down to chaos with two double-scroll structures ($s_3 \in (10.4, 14)$). Similarly, such dynamical characteristic occurs in Fig.4(b). Namely, the double-scroll attractor in 1-D MSCS can be extended only under certain parameter conditions. Obviously, the two parameters play a key role in the generation of multiple double-scroll structures.
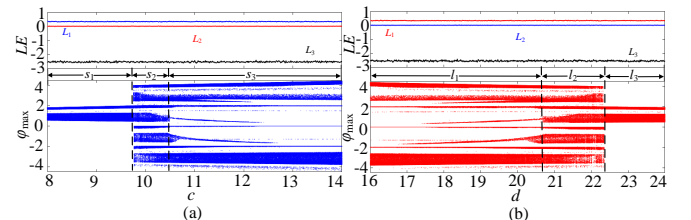
Fig. 4: Bifurcation diagram and first three Lyapunov exponents. (a) Dynamical behaviors related to parameter c. (b) Dynamical behaviors related to parameter d.

Next, the generation mechanism of 1-D MSCAs is analyzed. First, by letting $\dot{x} = \dot{y} = \dot{z} = \dot{\varphi} = 0$, the equilibrium points can be solved by

$$\begin{cases} a(y-f) = 0 \\ x - y + z = 0 \\ by = 0 \\ cx - dF = 0 \end{cases} \quad (14)$$

When keeping the original parameters a, b, m_0, and m_1 unchanged, setting relevant parameter $c=10$ and extension coefficient $d=21.8$, the solution of equilibrium equation (14) is obtained as

$$E = (x, y, z, \varphi) = \begin{cases} E_1 = (0, 0, 0, F(\varphi) = 0) \\ E_2 = (1.5, 0, -1.5, F(\varphi) = 0.6881) \\ E_3 = (-1.5, 0, 1.5, F(\varphi) = -0.6881) \end{cases} \quad (15)$$

Based on the above results, we can find that the equilibrium points in the x-, y-, and z-axis are unchanged compared with the basic Chua's system. In other words, the basic double-scroll attractor in phase space x-y-z is unchanged in this case. However, the original equilibrium points at the φ-axis are extended along three different functions including $F(\varphi)=0$, $F(\varphi)=0.6881$, and $F(\varphi)=-0.6881$, which results in the extension of the basic double-scroll attractor in the x-φ, y-φ, and z-φ planes, respectively. It should be particularly pointed out that the stability of all extension equilibrium points is identical with corresponding original equilibrium points since $d > 0$. Taking $M=1$ as an example, the distribution of the equilibrium points on the φ-x, φ-y, and φ-z planes are given in Fig.5(a1), (a2), and (a3), respectively. As we can see, under this case, the original equilibrium points are synchronously extended along the two opposite directions at the φ-axis with $F(\varphi)=0$, $F(\varphi)=0.6881$, and $F(\varphi)=-0.6881$. Meanwhile, the whole phase of the basic double-scroll in x-y-z space is also synchronously extended along the φ-axis, resulting in a 4-double-scroll chaotic attractor in x-φ, y-φ, and z-φ planes, as shown in Fig.5(a2), (b2), and (c2), respectively. To further verify the above analysis, the different numbers of double-scroll attractors are realized by setting $N=2$, 3, and $M=2$, 3, as shown in Fig.6. Clearly, arbitrary number ((odd number $2N+1$) and (even number $2M+2$)) of double-scroll attractors can be generated by choosing a suitable control parameter N/M.
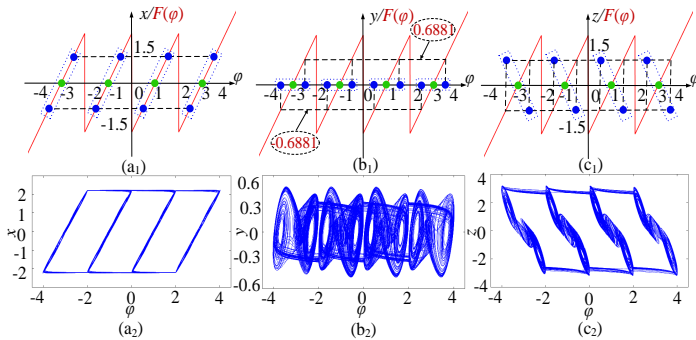

Fig. 5: Distribution of equilibrium points and corresponding phase trajectories of system (13) with $M=1$. (a1)-(a2) φ-x plane. (b1)-(b2) φ-y plane. (c1)-(c2) φ-z plane.
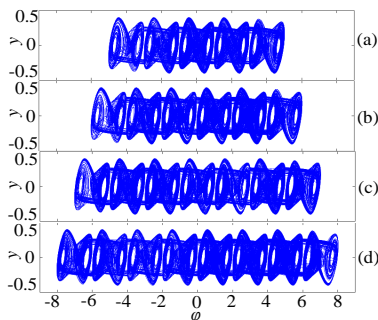

Fig. 6: 1-D MSCAs. (a) 5-double-scroll with $N=2$. (b) 6-double-scroll with $M=2$. (c) 7-double-scroll with $N=3$. (d) 8-double-scroll with $M=3$.
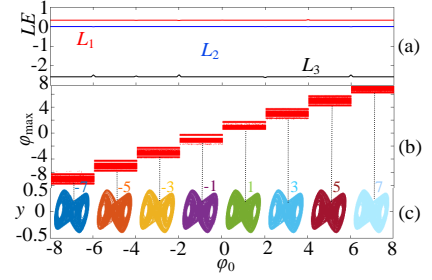

Fig. 7: Initial boosting behavior related to initial value φ_0 in the system (13). (a) First three Lyapunov exponents. (b) Bifurcation diagram. (c) Coexisting eight double-scroll attractors.

In addition, the constructed 1-D MSCS (13) can exhibit complex 1-D initial boosting behavior that is a complex dynamical behavior highly sensitive to initial states [35, 36]. For example, keeping the above parameter values unchanged except for $c=8$, $M=3$, and the initial value $\varphi_0 \in [-8, 8]$, Fig.7(a) shows the system produces continuously robust chaos because it has an invariant positive Lyapunov exponent. More important, the bifurcation diagram related to φ_0 in Fig.7(b) shows a typical initial boosting bifurcation phenomenon with stair-stepping diagram. In this case, each of the stair regions can evolve to be an attractor. That is to say, the system can generate a series of coexisting attractors with the same topology structure but different positions, which means the initial boosting behavior occurs. To further verify this characteristic, with $\varphi_0 = \pm 7$, ± 5, ± 3, ± 1, the phase portraits of coexisting eight chaotic double-scroll attractors can be generated along the φ-axis, as shown in Fig.7(c). A large number of simulations show that infinitely many coexisting double-scroll attractors can be obtained as N and M increase. This property is very significant in engineering applications because it can provide numerous nondestructive and robust chaotic signals with different offset amplitudes.

C. Designing 2-D MSCS Via Extending Two State Variables

Based on the UVEM, the system model of the 2-D MSCS can be described as

$$\begin{cases} \dot{x} = a(y-f) \\ \dot{y} = x - y + z \\ \dot{z} = by \\ \dot{\varphi}_1 = c_1 x - d_1 F_1(\varphi_1) \\ \dot{\varphi}_2 = c_2 y - d_2 F_2(\varphi_2) \end{cases} \quad (16)$$

where c_1, c_2, and d_1, d_2 are two sets of relevant parameters and extension coefficients, respectively. Next, the generation mechanism of 2-D MSCAs is analyzed. Letting $\dot{x} = \dot{y} = \dot{z} = \dot{\varphi}_1 = \dot{\varphi}_2 = 0$, the equilibrium points can be solved by

$$\begin{cases} a(y-f) = 0 \\ x - y + z = 0 \\ by = 0 \\ c_1 x - d_1 F_1 = 0 \\ c_2 y - d_2 F_2 = 0 \end{cases} \quad (17)$$

When keeping the original parameters a, b, m_0, and m_1 unchanged, and setting $c_1=10$, $d_1=21.8$, $c_2=24$, and $d_2=9$, the solution of equation (17) is given as

$$\begin{aligned} E &= (x, y, z, \varphi_1, \varphi_2) \\ &= \begin{cases} E_1 = (0, 0, 0, F_1(\varphi_1) = 0, F_2(\varphi_2) = 0) \\ E_2 = (1.5, 0, -1.5, F_1(\varphi_1) = 0.6881, F_2(\varphi_2) = 0) \\ E_3 = (-1.5, 0, 1.5, F_1(\varphi_1) = -0.6881, F_2(\varphi_2) = 0) \end{cases} \end{aligned} \quad (18)$$

The equilibrium points in (18) show that the original equilibrium points in x-y-z space are still unchanged. However, they are simultaneously extended at the φ_1- and φ_2-axis along four different functions including $F_1(\varphi_1) = F_2(\varphi_2) = 0$, $F_1(\varphi_1)=0.6881$, and $F_1(\varphi_1)=-0.6881$, which results in the extension of the basic double-scroll attractor in the φ_1-φ_2 plane. Similarly, the stability
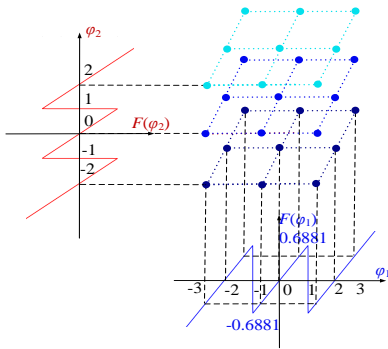
Fig. 8: Distribution of equilibrium points in the system (6) with $N_1=N_2=1$ on the φ_1-φ_2 plane.
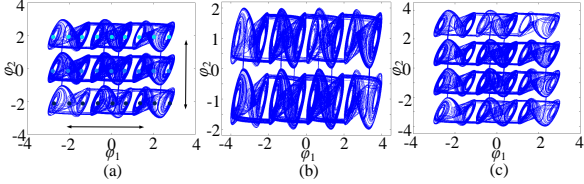

Fig. 9: 2-D MSCAs in φ_1-φ_2 plane. (a) 3x3-double-scroll attractor with $N_1=N_2=1$. (b) 4x2-double-scroll attractor with $M_1=1$, $M_2=0$. (c) 3x4-double-scroll attractor with $N_1=1$, $M_2=1$.

of all extension equilibrium points is identical to that of the corresponding basic equilibrium points since $d_1 > 0$ and $d_2 > 0$. Taking $N_1=N_2=1$ as an example, the distribution of the equilibrium points on the φ_1-φ_2 plane is given in Fig.8. As we can see in this case, the basic equilibrium points are synchronously extended along the two opposite directions at φ_1-axis and φ_2-axis with $F_1(\varphi_1)=F_2(\varphi_2)=0$, $F_1(\varphi_1)=0.6881$, and $F_1(\varphi_1)=-0.6881$. Meanwhile, the whole phase of the basic double-scroll attractor in x-y-z space is also simultaneously extended along φ_1- and φ_2-axis, resulting in a 3×3-double-scroll attractor in φ_1-φ_2 plane, as shown in Fig.9(a). Evidently, as the control parameters N_i/M_i (i=1, 2) increase, the basic double-scroll attractor is extended in the φ_1-φ_2 plane. To further verify the above analysis, 4×2-double-scroll and 3×4-double-scroll attractors are produced by setting ($M_1=1$, $M_2=0$) and ($N_1=1$, $M_2=1$), as shown in Fig.9(b) and (c), respectively. Therefore, arbitrary number $((2N_1+1)/(2M_1+2)\times(2N_2+1)/(2M_2+2))$ of 2-D MSCA can be generated by choosing suitable control parameters N_i/M_i.

Interestingly, the constructed 2-D MSCS (16) can exhibit complicated 2-D initial boosting behavior, which has not been reported in previous MSCSs. For example, when keeping the previous parameters unchanged except for c_1=8, c_2=20, $N_1=N_2=3$, the first three Lyapunov exponents and corresponding bifurcation diagrams with $\varphi_{10} \in$(-7,7) and $\varphi_{20} \in$(-7,7) are plotted in Fig.10(a) and (b), respectively. As we can see, both Fig.10(a) and Fig.10(b) show typical initial boosting bifurcation phenomena with stair-stepping diagram. In other words, system (16) simultaneously generates initial boosting behaviors along φ_{10}- and φ_{20}-directions, respectively, which means that 2-D initial boosting behavior occurs. For further verifying this feature, setting nine sets of different initial states (φ_{10}, φ_{20})=(-2/0/2, -2/0/2), the phase portraits of coexisting nine chaotic double-scroll attractors can be produced on the φ_1-φ_2 plane, as shown in Fig.11. It should be pointed that only partial coexisting attractors are given. In fact, infinitely many coexisting double-scroll attractors can be generated on φ_1-φ_2 plane as N_i and M_i increase. This property is very important in engineering applications since it can generate a series of nondestructive and robust chaotic signals with different offset amplitudes along two different directions.

IV. MWCSs BASED ON LORENZ SYSTEM

This section designs Lorenz system-based 1-D and 2-D MWCSs using UVEM, discusses their chaos mechanisms and analyzes their dynamical behaviors.
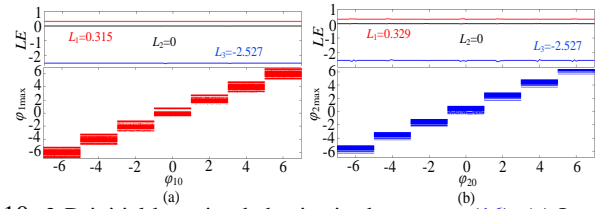
A. Brief Description of the Lorenz system

Fig. 10: 2-D initial boosting behavior in the system (16). (a) Lyapunov exponents and bifurcation diagram related to φ_{10}. (b) Lyapunov exponents and bifurcation diagram related to φ_{20}.
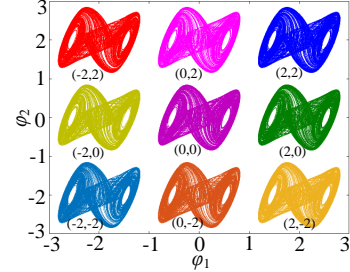

Fig. 11: Coexisting nine double-scroll attractors in φ_1-φ_2 plane.

The original model of the Lorenz system can be expressed as [37]

$$\begin{cases} \dot{x} = \alpha(y-x) \\ \dot{y} = \beta x - y - xz \\ \dot{z} = xy - \gamma z \end{cases} \quad (19)$$

When the parameters α=10, β=28, γ=8/3, and initial states are (0.1, 0.1, 0.1), the system (19) can generate typical double-wing chaotic attractors with one unstable saddle point (P_2) and two indexe-2 saddle-focus (P_1 and P_3), as shown in Fig.12.
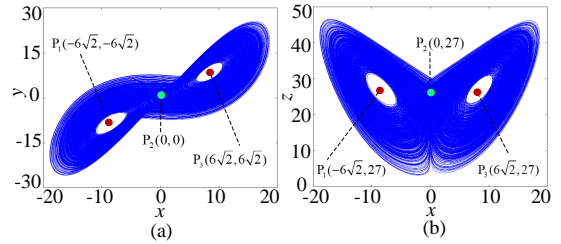

Fig. 12: Double-wing attractor of the system (19). (a) x-y plane. (b) x-z plane.

B. Designing 1-D MWCS Via Extending One State Variable

According to the UVEM, a 1-D MWCS is constructed as follows

$$\begin{cases} \dot{x} = \alpha(y-x) \\ \dot{y} = \beta x - y - xz \\ \dot{z} = xy - \gamma z \\ \dot{\varphi} = cx - dF \end{cases} \quad (20)$$

Letting $\dot{x} = \dot{y} = \dot{z} = \dot{\varphi}$=0, the relevant parameter c=1, the extension coefficient d=15.4, the equilibrium points can be solved as follows

$$E = (x,y,z,\varphi) = \begin{cases} E_1 = (0,0,0,F(\varphi) = 0) \\ E_2 = (6\sqrt{2},6\sqrt{2},27,F(\varphi) = 0.551) \\ E_3 = (-6\sqrt{2},-6\sqrt{2},27,F(\varphi) = -0.551) \end{cases} \quad (21)$$

From equation (21), the original equilibrium points in the x-, y-, and z-axis are unchanged. Nevertheless, the equilibrium points are extended along the φ-axis with three different functions including $F(\varphi)$=0, $F(\varphi)$=0.551, and $F(\varphi)$=-0.551, which results in the extension of the basic double-wing attractor in the x-φ, y-φ, and z-φ planes, respectively. Taking M=1 as an example, the distribution of equilibrium points in x-φ, y-φ, and z-φ planes is given in Fig.13(a1), (b1), and (c1), respectively. Clearly, the whole phase of the basic double-wing attractor is extended in x-φ, y-φ, and z-φ planes, resulting in the generation of a 4-double-wing attractor, as shown in Fig.13(a2), (b2), and (c2), respectively. That is to say, as N/M increases, the basic double-wing attractor is extended along the two opposite directions at
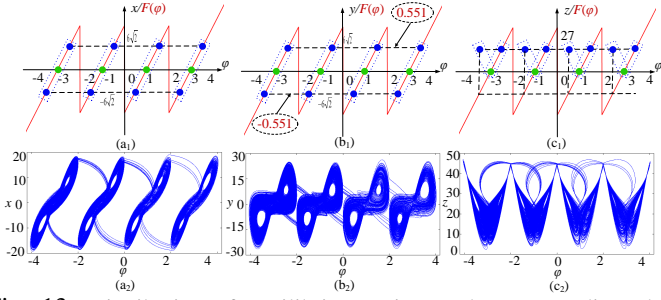
Fig. 13: Distribution of equilibrium points and corresponding phase trajectories of system (20) with M=1. (a1)-(a2) φ-x plane. (b1)-(b2) φ-y plane. (c1)-(c2) φ-z plane.
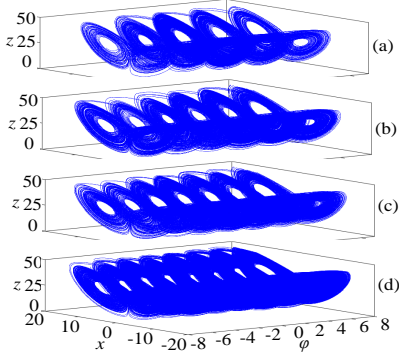

Fig. 14: 1-D MWCAs. (a) 5-double-wing attractor. (b) 6-double-wing attractor. (c) 7-double-wing attractor. (d) 8-double-wing attractor.

the φ-axis. To further verify the above analysis, Fig.14 gives the phase portrait of 5-, 6-, 7-, and 8-double-wing chaotic attractors with control parameters N=2, M=2, N=3, and M=3, respectively.

Similarly, the presented 1-D MWCS (20) can exhibit 1-D initial boosting behavior. To better display this coexisting behavior distributed on the initial plane, the local basin of attraction for c=0.8, d=15.4, and M=3 on the x_0-φ_0 plane is plotted in Fig.15(a). As can be seen, the basin of attraction has eight different regions painted with different colors. Here each region stands for the attraction regions of chaotic attractors with different positions. That is to say, the 1-D MWCS (20) can generate a series of coexisting chaotic attractors with different positions under different values of φ_0. To further verify this characteristic, with φ_0=±7, ±5, ±3, ±1, coexisting eight chaotic double-wing attractors are generated along the φ-axis, as shown in Fig.15(b). Numerous simulations show that infinitely many coexisting double-wing attractors can be obtained with $N/M \to \infty$. Therefore, the 1-D MWCS (20) exhibits significant 1-D initial boosting behavior.
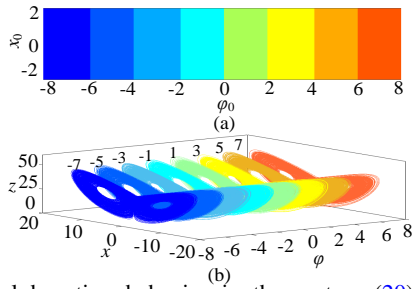

Fig. 15: Initial boosting behavior in the system (20). (a) Basin of attraction related to φ_0 and x_0 values. (b) Coexisting eight double-wing attractors in φ-x-z phase space.

C. Designing 2-D MWCS Via Extending Two State Variables

Based on the UVEM, the 2-D MWCS can be constructed as

$$
\begin{cases}
\dot{x} = \alpha(y-x) \\
\dot{y} = \beta x - y - xz \\
\dot{z} = xy - \gamma z \\
\dot{\varphi}_1 = c_1 x - d_1 F_1 \\
\dot{\varphi}_2 = c_2 y - d_2 F_2
\end{cases}
\tag{22}
$$

Letting c_1=1, d_1=15.4, c_2=1, d_2=22, $\dot{x}=\dot{y}=\dot{z}=\dot{\varphi}_1=\dot{\varphi}_2=0$, the equilibrium points can be solved as follows

$$
\begin{aligned}
&E = (x,y,z,\varphi_1,\varphi_2) = \\
&\begin{cases}
E_1 = (0,0,0,F(\varphi_1)=0,F(\varphi_2)=0) \\
E_2 = (6\sqrt{2},6\sqrt{2},27,F(\varphi_1)=0.551,F(\varphi_2)=0.3857) \\
E_3 = (-6\sqrt{2},-6\sqrt{2},27,F(\varphi_1)=-0.551,F(\varphi_2)=-0.3857)
\end{cases}
\end{aligned}
\tag{23}
$$

From Equation (23), the basic equilibrium points are still unchanged in this case. However, they are synchronously extended at φ_1- and φ_1-axis, respectively, along six different functions $F(\varphi_1)$=0, $F(\varphi_2)$=0, $F(\varphi_1)$=0.551, $F(\varphi_1)$=-0.551, $F(\varphi_2)$=0.3857, and $F(\varphi_2)$=-0.3857. Such behavior causes the extension of phase space of the basic double-wing attractor in the φ_1-φ_2 plane. For example, when N_1=N_2=1, the distribution of equilibrium points of system (22) is plotted in Fig.16. Obviously, the original equilibrium points are synchronously extended along the two opposite directions of the φ_1-axis and φ_2-axis. Meanwhile, the whole phase space of the basic double-wing is also simultaneously extended along φ_1- and φ_2-axis, resulting in a 3×3-double-wing chaotic attractor in the φ_1-φ_2 plane, as shown in Fig.17(a). Therefore, the system (22) can generate an arbitrary number of 2-D MWCAs, as shown in Fig.17.

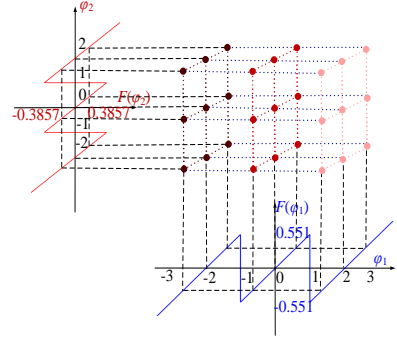Fig. 16: Distribution of equilibrium points in the system (22) with N_1=N_2=1 on the φ_1-φ_2 plane.
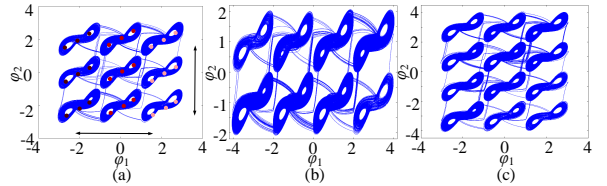

Fig. 17: 2-D MWCAs on the φ_1-φ_2 plane. (a) 3×3-double-wing attractor with N_1=N_2=1. (b) 4×2-double-wing attractor with M_1=1, M_2=0. (c) 3×4-double-wing attractor with N_1=M_2=1.

Similarly, the 2-D MWCS (22) can exhibit 2-D initial boosting behavior, which has not been reported in previous MWCSs. To verify this property, we plot the local basin of attraction for c_1=0.8, d_1=15.4, c_2=0.8, d_2=22, and N_1=N_2=1 in the φ_{10}-φ_{20} plane and show the results in Fig.18(a). It can be seen that the basin of attraction has nine different regions painted with different colors. Clearly, the initial boosting behavior occurs along φ_1 and φ_2 directions, simultaneously, which shows the 2-D initial boosting behavior occurs. Thus, the system (22) can generate a series of coexisting chaotic attractors with different positions in the φ_1-φ_2 plane. Taking (φ_{10}, φ_{20})=(-2/0/2, -2/0/2) as an example, coexisting nine chaotic double-wing attractors can be obtained in the φ_1-φ_2 plane, as shown in Fig.18(b). Therefore, the constructed 2-D MWCS (22) has complex 2-D initial boosting behavior.

V. HARDWARE IMPLEMENTATION

Recently, FPGA-based chaotic circuit implementation has attracted much attention due to its high stability, fast calculation, and ease of changing system parameters and initial values [38]. To demonstrate the simplicity of UVEM in hardware implementation,
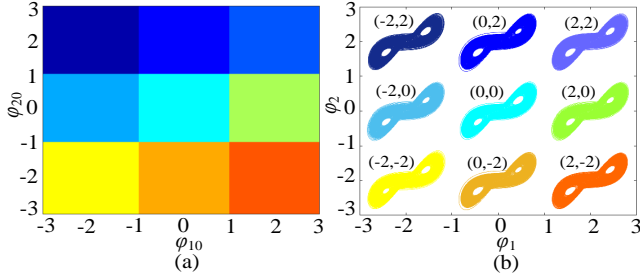
Fig. 18: Initial boosting behavior in the system (22). (a) Basin of attraction related to φ_{10} and φ_{20} values. (b) Coexisting nine double-wing attractors.
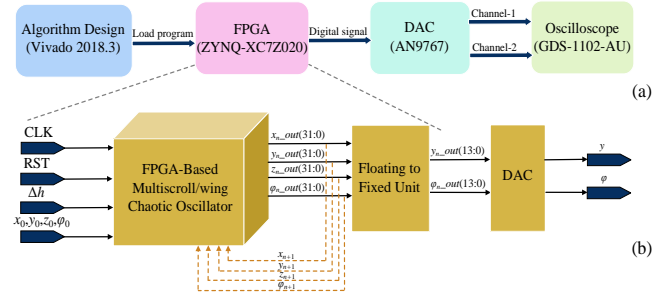

Fig. 19: FPGA-based digital circuit implementation. (a) The block diagram of the hardware experiment. (b) The flow diagram of the chaotic system implementation.

this section implements the designed 1-D and 2-D MS/WCSs using FPGA technology. Usually, the FPGA-based realization of chaotic systems mainly includes three parts: algorithm design, hardware planning, and experimental measurement.

A. Algorithm Design

First, in this subsection, the designed MS/WCSs are discretized by using numerical algorithms. At present, many numerical algorithms such as the Runge-Kuntta algorithm, Euler algorithm, and the Heun algorithm can be used to solve the nonlinear differential equations of chaotic systems [39]. In this paper, a fourth-order Runge-Kutta (RK-4) algorithm is adopted due to its high accuracy and easy realization. Taking the 1-D MSCS in system (13) as an example, discretization is presented by using the RK-4 method. Based on chaotic system (13), we can deduce

$$\begin{cases} K_{x1} = a(y(n) - f(x(n))) \\ K_{y1} = x(n) - y(n) + z(n) \\ K_{z1} = by(n) \\ K_{\varphi1} = cx(n) - dF(\varphi(n)) \end{cases} \quad (24)$$

where $x(n)$, $y(n)$, $z(n)$, and $\varphi(n)$ are the n-th sampling values of state variables x, y, z, and φ, respectively. We then have

$$\begin{cases} K_{x2} = a((y(n) + 0.5\Delta hK_{y1}) - f(x(n) + 0.5\Delta hK_{x1})) \\ K_{y2} = (x(n) + 0.5\Delta hK_{x1}) - (y(n) + 0.5\Delta hK_{y1}) + (z(n) + 0.5\Delta hK_{z1}) \\ K_{z2} = b(y(n) + 0.5\Delta hK_{y1}) \\ K_{\varphi2} = c(x(n) + 0.5\Delta hK_{x1}) - dF(\varphi(n) + 0.5\Delta hK_{\varphi1}) \end{cases} \quad (25)$$

Further we get

$$\begin{cases} K_{x3} = a((y(n) + 0.5\Delta hK_{y2}) - f(x(n) + 0.5\Delta hK_{x2})) \\ K_{y3} = (x(n) + 0.5\Delta hK_{x2}) - (y(n) + 0.5\Delta hK_{y2}) + (z(n) + 0.5\Delta hK_{z2}) \\ K_{z3} = b(y(n) + 0.5\Delta hK_{y2}) \\ K_{\varphi3} = c(x(n) + 0.5\Delta hK_{x2}) - dF(\varphi(n) + 0.5\Delta hK_{\varphi2}) \end{cases} \quad (26)$$

Finally we have

$$\begin{cases} K_{x4} = a((y(n) + \Delta hK_{y3}) - f(x(n) + \Delta hK_{x3})) \\ K_{y4} = (x(n) + \Delta hK_{x3}) - (y(n) + \Delta hK_{y3}) + (z(n) + \Delta hK_{z3}) \\ K_{z4} = b(y(n) + \Delta hK_{y3}) \\ K_{\varphi4} = c(x(n) + \Delta hK_{x3}) - dF(\varphi(n) + \Delta hK_{\varphi3}) \end{cases} \quad (27)$$

By combining equations (24)-(27), the discrete system of the 1-D MSCS can be established as

$$\begin{cases} x(n+1) = x(n) + \Delta h(K_{x1} + 2K_{x2} + 2K_{x3} + K_{x4})/6 \\ y(n+1) = y(n) + \Delta h(K_{y1} + 2K_{y2} + 2K_{y3} + K_{y4})/6 \\ z(n+1) = z(n) + \Delta h(K_{z1} + 2K_{z2} + 2K_{z3} + K_{z4})/6 \\ \varphi(n+1) = \varphi(n) + \Delta h(K_{\varphi1} + 2K_{\varphi2} + 2K_{\varphi3} + K_{\varphi4})/6 \end{cases} \quad (28)$$

where $x(n+1)$, $y(n+1)$, $z(n+1)$, and $\varphi(n+1)$ are the $(n+1)$-th sampling values of state variables x, y, z, and φ, respectively. Δh is the sampling step, K_{xi}, K_{yi}, K_{zi}, and $K_{\varphi i}$ (i=1,2,3,4) are temporary variables.

B. Hardware Planning

Next, in this subsection, the discrete MS/WCSs are implemented by using FPGA technology. Fig.19(a) gives the basic block diagram of the hardware experiment based on FPGA, where the Vivado 2018.3 tool is used as the design and simulation platform, the Xilinx ZYNQ-XC7Z020 chip is adopted in FPGA, the

AN9767 is used as the digital-to-analog converter (DAC) module and a dual-channel digital oscilloscope GWINSTEK GDS-1102-AU is employed to observe and capture the experimental results.

The discretized MS/WCSs are realized in the Vivado design suite using the Verilog HDL language. Where the discretization step $\triangle h$ is 0.001 and the IEEE 754-1985 high precision 32-bit floating point standard is adopted. The key flow diagram of the algorithm implementation in FPGA is shown in Fig.19(b). As can be seen, there are three modules: chaotic oscillator, floating-to-fixed unit, and DAC unit. The chaotic oscillator module mainly uses the RK-4 algoritHM to solve the MS/WCSs. It contains four input signals and five output signals, where the system clock "CLK" and the reset signal "RST" are two 1-bit control signals, $\triangle h$ and the initial values (x_0, y_0, z_0, φ_0) are both 32-bit input signals. The four 32-bit output signals (x_{n_out}, y_{n_out}, z_{n_out}, φ_{n_out}) are used as the initial values of the next iteration of the chaotic oscillator. These signals are equivalent to the x, y, z, and φ variables of the 1-D MSCS. Meanwhile, they are also input to the floating to fixed unit and are further converted into a 14-bit fixed-point number. In particular, considering the phase portraits on φ-y planes and to save hardware resources, only two 14-bit output signals are implemented.

Additionally, to better exhibit their connected relationship, Fig.20 gives a hierarchical structure of the Verilog HDL program for the FPGA-based implementation of the 1-D MSCS. First, the discretized differential equations of chaotic systems are described by using various intellectual property (IP) cores including adder, subtractor, multiplier, exponent, and absolute value in the Vivado compilation environment. The entire logic circuits are initialized by the main controller when the experiment board is turned on, and they begin iterating over the initial states of $x(n)$, $y(n)$, $z(n)$, and $\varphi(n)$. Then, the discretized equations (four function units Fx, Fy, Fz, $F\varphi$) are constructed using the IP instances. The main controller carries out the four-time loading sequences of F=[Fx, Fy, Fz, $F\varphi$] and switches the subsequences of K_i=[K_{xi}, K_{yi}, K_{zi}, $K_{\varphi i}$] (i=1,2,3,4) using the cycle counter. By weighing the results of the calculation, $Y(n+1)$=[$x(n+1)$, $y(n+1)$, $z(n+1)$, $\varphi(n+1)$] can then be obtained. Finally, the floating-point numbers are converted into 14-bit integers and further converted into analog signals through the DAC module. The output analog signals can be observed via an oscilloscope.

C. Experimental Measurement

According to the above design process, the MS/WCSs including systems (13), (16), (20), and (22) are physically implemented. The hardware experimental devices including a Lenovo laptop E490 with Intel CoreTM i7 CPU 2.500GHz, an FPGA development board, and a digital oscilloscope are shown in Fig.21. Fig.22 gives 1-D- and 2-D-MS/WCAs captured by the digital oscilloscope. It is worth noting that the experimentally captured results are in agreement with those of Fig.6, Fig.9, Fig.14, and Fig.17 obtained from the Matlab platform. This shows the correctness and feasibility of the hardware design based on FPGA and also provides proof of the proposed UVEM.
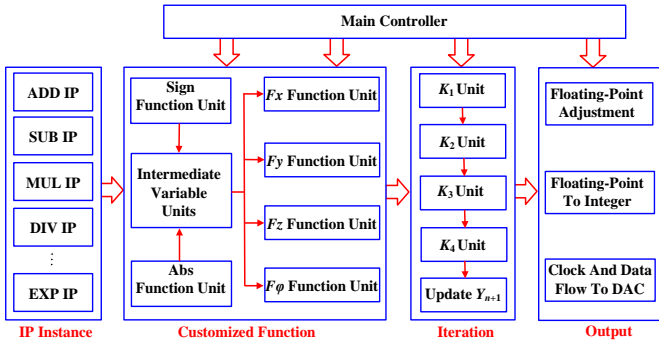
Fig. 20: Hierarchical structure of Verilog HDL program for FPGA-based implementation.
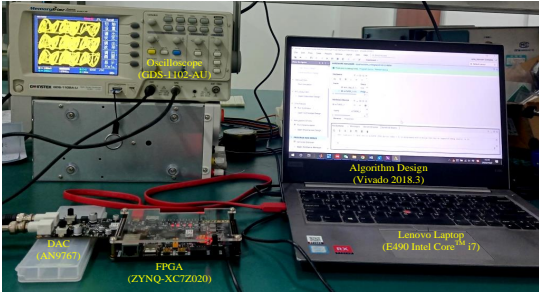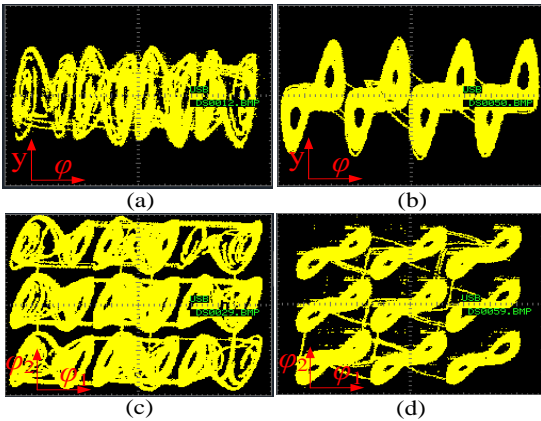

Fig. 21: Hardware implementation devices

Fig. 22: FPGA-based experiment results. (a) 1-D 4-double-scroll attractor. (b) 1-D 4-double-wing attractor. (c) 2-D 3×3-double-scroll attractor. (d) 2-D 3×3-double-wing attractor.

VI. COMPARISION AND APPLICATION

A. Comparison analysis

It should be particularly noted that the UVEM is a universal one and can be applied in arbitrary double-scroll/wing chaotic systems. For instance, the generation of 1-D and 2-D MS/WCSs from the Jerk system [9], Sprott system [40], and Chen system [41] is shown in Table II. It is noted that in the table the abbreviations "Sytem" and "Para." show the words "Systems" and "Parameters", respectively. In Table II, the first column is the original double-scroll/wing systems. By adopting the UVEM, the corresponding 1-D MS/WCSs can be implemented as shown in the second column. The fourth column shows the corresponding chaotic attractors under fixed parameter values given in the third column. Similarly, the 2-D MS/WCSs can be constructed by using UVEM as shown in the fifth column. And the corresponding chaotic attractors are given in the last column. Obviously, by using UVEM, both 1-D MS/WCSs and 2-D MS/WCSs can be realized easily.

Table III compares the UVEM with current existing design methods of MS/WCSs. As observed from Table III, all of the existing methods can only be applied to construct MSCSs or

MWCSs. That is to say, they are not universal. Unlike these traditional design methods, the UVEM has universality. By using the same steps and the same nonlinear control functions, both MSCSs and MWCSs can be constructed. Moreover, the UVEM enjoys some advantages in terms of basic systems, control parameters, and dynamical behaviors. For example, in traditional methods, the basic double-scroll/wing systems must be changed. In most existing methods [4, 18, 24, 29], the control parameters are non-integral, which makes it very difficult to adjust chaotic attractors. on the contrary, the UVEM is no need to change the original basic systems and only requires integer parameters. More importantly, the MS/WCSs designed by UVEM can exhibit both 1-D and 2-D initial boosting behaviors. The one small pity is that the UVEM can not apply to generate 3-D MS/WCAs. To sum up, the UVEM has the characteristic of universality, simple implementation, easy control, and complex dynamcis. Arbitrary customized MS/WCSs with different attractors can be obtained to meet the different application requirements.

B. Application in PRNG

In engineering applications, chaotic systems are usually applied to design pseudorandom number generators (PRNGs) [42]. The PRNG is widely applied in various industrial fields such as computers, digital signatures, communication, and information encryption [7, 36, 43]. Since the MS/WCSs can generate chaotic sequences with complex dynamics, they can achieve good performance in this application. Here, we design random number generators using the multi-scroll/wing chaotic sequences, which are produced by the 1-D and 2-D MS/WCSs in (13), (16), (20), and (22). Firstly, a chaotic sequence $S=(s_1, s_2, \ldots, s_n, \ldots)$ is generated by the MS/WCSs. Then, each value s_n in S is transformed into a 32-bit stream according to the IEEE 754 standard. Finally, the 17th-32nd bits from the bit stream are truncated as pseudorandom numbers. The designed PRNG can be described as

$$P_i = B(s_n)_{17:32} \qquad (29)$$

where $B(.)$ is to transform a value into a 32-bit float number obeying the IEEE floating point standard, and P is the obtained random number sequence. Hence, sixteen bits numbers are produced for each output of the chaotic sequence. The random numbers are expected to have high randomness. The NIST SP800-22 is used to test the random numbers [44]. It is a convinced and all-side test standard that contains 15 sub-tests. According to the setting and requirements, we set the significance level as 0.01, and the test binary sequences are of length 10^6 bits. Then a total number of 152 binary sequences are generated and tested.

In our experiments, we first generate four chaotic sequences with length 10^7 from the four different MS/WCSs, and then produce 160 binary sequences with 10^6 bits. To obtain more neutral test results, the first 8 binary sequences are discarded and the remaining 152 binary sequences are used for testing. The value of a P-valueT larger than 0.01 is considered to pass the related sub-test. Table IV lists the test results of the four sets of chaotic sequences generated by the MS/WCSs. We can see that they can pass all the sub-tests of the NIST SP800-22 test suite. This means that the MS/WCSs produce random numbers with high randomness.

VII. CONCLUSION

In this paper, we have proposed a novel UVEM to construct MS/WCSs. It is a simple and universal construction method and can generate 1-D and 2-D MS/WCSs with multi-scroll/wing attractors. Theoretical analysis shows that the UVEM can be applied to any double-scroll/wing chaotic system, which is obviously different from the existing methods. Furthermore, the UVEM does not change the original double-scroll/wing chaotic systems and only requires extending new state variables. Based

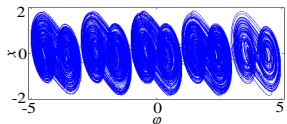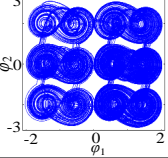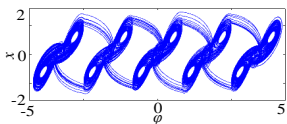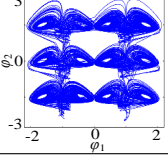TABLE II: DESIGN OF 1D- AND 2D-MS/WCSs BASED DS/WCS FAMILY
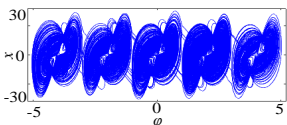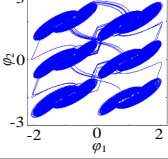
Sytem	1-D MS/WCSs	Para.	1-D MS/WCAs	2-D MS/WCSs	Para.	2-D MS/WCAs
Jerk	$\begin{cases}\dot{x}=y\\\dot{y}=z\\\dot{z}=-y-0.6z+\mathrm{sgn}(x)-x\\\dot{\varphi}=cx-dF(\varphi)\end{cases}$	$c=1.0$ $d=2.2$ $N=2$		$\begin{cases}\dot{x}=y\\\dot{y}=z\\\dot{z}=-y-0.6z+\mathrm{sgn}(x)-x\\\dot{\varphi}_1=c_1x-d_1F(\varphi_1)\\\dot{\varphi}_2=c_2y-d_2F(\varphi_2)\end{cases}$	$c_1=1.0$ $d_1=2.2$ $c_2=1.7$ $d_2=2.5$ $M_1=0$ $N_2=1$	
Sprott	$\begin{cases}\dot{x}=2(z-x)\\\dot{y}=0.4-z^2\\\dot{z}=8xy\\\dot{\varphi}=cx-dF(\varphi)\end{cases}$	$c=2.8$ $d=2.6$ $N=2$		$\begin{cases}\dot{x}=2(z-x)\\\dot{y}=0.4-z^2\\\dot{z}=8xy\\\dot{\varphi}_1=c_1x-d_1F(\varphi_1)\\\dot{\varphi}_2=c_2y-d_2F(\varphi_2)\end{cases}$	$c_1=2.8$ $d_1=2.6$ $c_2=2.8$ $d_2=2.0$ $M_1=0$ $N_2=1$	
Chen	$\begin{cases}\dot{x}=35(y-x)\\\dot{y}=-7x+28y-xz\\\dot{z}=xy-3z\\\dot{\varphi}=cx-dF(\varphi)\end{cases}$	$c=1.0$ $d=18$ $N=2$		$\begin{cases}\dot{x}=35(y-x)\\\dot{y}=-7x+28y-xz\\\dot{z}=xy-3z\\\dot{\varphi}_1=c_1x-d_1F(\varphi_1)\\\dot{\varphi}_2=c_2y-d_2F(\varphi_2)\end{cases}$	$c_1=1.0$ $d_1=18$ $c_2=1.0$ $d_2=22$ $M_1=0$ $N_2=1$	

TABLE III: COMPARISON OF DIFFERENT MS/WCS DESIGN METHODS.

References.	Methods	Universality	Changing basic system	Control parameters	Attractor dimension	Initial boosting behavior
2019 (MWCS) [24]	Pulse control	No	Yes	Non-integer	1-, 2-, 3-D	No
2020 (MSCS) [4]	nonlinear function control	No	Yes	Non-integer	1-D	No
2021 (MWCS) [18]	Sinusoidal function control	No	Yes	Non-integer	1-D	1-D
2021 (MSCS) [3]	Memristor coupling	No	Yes	Integer	1-D	1-D
2022 (MSCS) [29]	Fractal transformation	No	Yes	Non-integer	1-D	No
This work(MS/WCSs)	UVEM	Yes	No	Integer	1-, 2-D	1-, 2-D

TABLE IV: NIST STATISTICAL TEST RESULTS OF THE DESIGNED PRNG

No.	Sub-tests	P-valueT 1-D MSCS	P-valueT 2-D MSCS	P-valueT 1-D MWCS	P-valueT 2-D MWCS
01	Frequency	0.1321	0.6440	0.2622	0.5169
02	Block Frequency	0.4325	0.5157	0.7129	0.8729
03	Cum.Sums*(F)	0.7399	0.9428	0.9891	0.1718
	Cum.Sums*(R)	0.3613	0.1986	0.8165	0.2803
04	Runs	0.1596	0.9934	0.2368	0.9934
05	Longest Runs	0.6993	0.6579	0.5075	0.9558
06	Rank	0.3397	0.5612	0.3293	0.9615
07	FFT	0.1916	0.1537	0.6855	0.4140
08	Non-Ovla.Temp.*	0.3814	0.5476	0.3838	0.3725
09	Ovla.Temp.	0.0855	0.5075	0.7918	0.5886
10	Universal	0.7399	0.0891	0.9280	0.4190
11	Appr.Entropy	0.4559	0.0497	0.1005	0.0456
12	Ran.Exc.*	0.4392	0.7273	0.4580	0.6267
13	Ran.Exc.Var.*	0.3972	0.5216	0.3241	0.6059
14	Serial (1st)	0.6163	0.9199	0.4814	0.5476
	Serial (2nd)	0.9280	0.4190	0.1782	0.8400
15	Linear Complexity	0.6579	0.4685	0.1596	0.6301

on Chua's system and Lorenz system, two examples of designing MS/WCSs are studied to demonstrate the effectiveness and universality of UVEM. The chaos mechanism and dynamical behavior of the designed MS/WCSs are analyzed using basic dynamics methods. The research results show that multi-scroll/wing chaotic attractors can be obtained and their number can be controlled by a few integer parameters. Moreover, the MS/WCSs designed by UVEM exhibit 1-D and 2-D initial boosting behaviors. FPGA-based hardware experiment is further given to prove the simplicity of UVEM in physical implementation. Finally, to show the application of MS/WCSs, we designed a PRNG based on the proposed MS/WCSs. The test results demonstrate that the designed PRNG has high randomness. Undoubtedly, this work provides a perfect solution to construct different MS/WCSs, which may further reduce their design cost and promote their application in different fields. Besides, part of 3-D MS/WCSs can also be implemented by UVEM, which is what we need to further investigate in the future.

REFERENCES

[1] Z. Hua, B. Zhou, Y. Zhou, "Sine chaotification model for enhancing chaos and its hardware implementation," *IEEE Trans. Ind. Electron.*, vol. 66, no. 2, pp. 1273-1284, 2019.

[2] M. Ji'e, D. Yan, S. Sun, et al, "A simple method for constructing a family of Hamiltonian conservative chaotic systems," *IEEE Trans. Circuits Syst. I-Regul. Pap.*, vol. 69, no. 8, pp. 3328-3338, 2022.

[3] S. Zhang, C. Li, J. Zheng, et al, "Generating any number of initial offset-boosted coexisting chua's double-scroll attractors via piecewise-nonlinear memristor," *IEEE Trans. Ind. Electron.*, vol. 69, no. 7, pp. 7202-7212, 2021.

[4] N. Wang, G. Zhang, H. Li, "Parametric control for multi-scroll attractor generation via nested sine-PWL function," *IEEE Trans. Circuits Syst. II-Express Briefs.*, vol. 68, no. 3, pp. 1033-1037, 2022.

[5] S. Sahoo, B. K. Roy, "Design of multi-wing chaotic systems with higher largest Lyapunov exponent," *Chaos Solitons Fractals.*, vol. 157, p. 111926, 2022.

[6] N. Yu, Y. Wang, X. Liu, et al, "3D grid multi-wing chaotic attractors," *Int. J. Bifurcation Chaos.*, vol. 28, no. 04, p. 1850045, 2018.

[7] X. Liu, X. Tong, Z. Wang, et al, "Construction of controlled multi-scroll conservative chaotic system and its application in color image encryption," *Nonlinear Dyn.*, vol. 110, no. 2, pp. 1897-1934, 2022.

[8] J. Suykens, J. Vandewalle, "Quasilinear approach to nonlinear systems and the design of n-double scroll, no. n= 1, 2, 3, 4,...)," *IEE Proceedings G (Circuits, Devices and Systems)*, vol. 138, no. 5, pp. 595-603, 1991.

[9] S. Yu, J. Lü, H. Leung, et al, "Design and implementation of n-scroll chaotic attractors from a general jerk circuit," *IEEE Trans. Circuits Syst. I-Regul. Pap.*, vol. 52, no. 7, pp. 1459-1476, 2005.

[10] S. Yu, W. K. S. Tang, J. Lü, et al, "Generation of nxm-wing Lorenz-like attractors from a modified Shimizu-Morioka model," *IEEE Trans. Circuits Syst. II-Express Briefs.*, vol. 55, no. 11, pp. 1168-1172, 2008.

[11] S. Yu, W. K. S. Tang, J. Lü, et al, "Design and implementation of multi-wing butterfly chaotic attractors via Lorenz-type systems," *Int. J. Bifurcation Chaos.*, vol. 20, no. 01, pp. 29-41, 2010.

[12] S. Yu, J. Lü, G. Chen, et al, "Design and implementation of grid multiwing butterfly chaotic attractors from a piecewise Lorenz system," *IEEE Trans. Circuits Syst. II-Express Briefs.*, vol. 57, no. 10, pp. 803-807, 2010.

[13] S. Yu, J. Lü, X. Yu, et al, "Design and implementation of grid multiwing hyperchaotic Lorenz system family via switching control and constructing super-heteroclinic loops," *IEEE Trans. Circuits Syst. I, Reg. Papers.*, vol. 59, no. 5, pp. 1015-1061, 2012.

[14] Y. Huang, P. Zhang, W. Zhao, "Novel grid multiwing butterfly chaotic attractors and their circuit design," *IEEE Trans. Circuits Syst. II-Express Briefs.*, vol. 62, no. 5, pp. 496-500, 2015.

[15] F. R. Tahir, S. Jafari, V. T. Pham, et al, "A novel no-equilibrium chaotic system with multiwing butterfly attractors," *Int. J. Bifurcation Chaos.*, vol. 25, no. 04, p. 1550056, 2015.

[16] C. Wang, X. Liu, H. Xia, "Multi-piecewise quadratic nonlinearity memristor and its 2N-scroll and 2N+1-scroll chaotic attractors system," *Chaos.*, vol. 27, no. 3, p. 033114, 2017.

[17] K. Rajagopal, S. Çiçek, P. Naseradinmousavi, et al, "A novel parametrically controlled multi-scroll chaotic attractor along with electronic circuit design," *Eur. Phys. J. Plus.*, vol. 133, no. 9, pp. 1-8, 2018.

[18] H. Lin, C. Wang, F. Yu, et al, "An extremely simple multiwing chaotic system: dynamics analysis, encryption application, and hardware implementation," *IEEE Trans. Ind. Electron.*, vol., 68, no. 12, pp. 12708-12719, 2020.

[19] N. Wang, G. Zhang, N. V. Kuznetsov, et al, "Generating grid chaotic sea from system without equilibrium point," *Commun. Nonlinear Sci. Numer. Simul.*, vol. 107, p. 106194, 2022.

[20] Q. Hong, Q. Wu, X. Wang, et al, "Novel nonlinear function shift method for generating multiscroll attractors using memristor-based control circuit," *IEEE Trans. Very Large Scale Integr. (VLSI) Syst.*, vol. 27, no. 5, pp. 1174-1185, 2019.

[21] F. Zaamoune, T. Menacer, R. Lozi, et al, "Symmetries in hidden bifurcation routes to multiscroll chaotic attractors generated by saturated function series," *Journal of Advanced Engineering and Computation.*, vol. 3, no. 4, pp. 511-522, 2019.

[22] Y. Yang, L. Huang, J. Xiang, et al, "Three-dimensional sine chaotic system with multistability and multi-scroll attractor," *IEEE Trans. Circuits Syst. II-Express Briefs.*, vol. 69, no. 3, pp. 1792-1796, 2021.

[23] R. J. Escalante-González, E. Campos-Cantón, "A class of piecewise linear systems without equilibria with 3-D grid multiscroll chaotic attractors," *IEEE Trans. Circuits Syst. II-Express Briefs.*, vol. 66, no. 8, pp. 1456-1460, 2018.

[24] Q. Hong, Y. Li, X. Wang, et al, "A versatile pulse control method to generate arbitrary multidirection multibutterfly chaotic attractors," *IEEE Trans. Comput-Aided Des. Integr. Circuits Syst.*, vol. 38, no. 8, pp. 1480-1492, 2019.

[25] Q. Wu, Q. Hong, X. Liu, et al, "Constructing multi-butterfly attractors based on Sprott C system via non-autonomous approaches," *Chaos.*, vol. 29, no. 4, p. 043112, 2019.

[26] N. Wang, C. Li, H. Bao, et al, "Generating multi-scroll Chua's attractors via simplified piecewise-linear Chua's diode," *IEEE Trans. Circuits Syst. I-Regul. Pap.*, vol. 66, no. 12, pp. 4767-4779, 2019.

[27] S. Zhang, C. Li, J. Zheng, et al, "Generating any number of diversified hidden attractors via memristor coupling," *IEEE Trans. Circuits Syst. I-Regul. Pap.*, vol., 68, no. 12, pp. 4945-4956, 2021.

[28] A. Azam, M. Aqeel, D. A. Sunny, "Generation of multidirectional mirror symmetric multiscroll chaotic attractors (MSMCA) in double wing satellite chaotic system," *Chaos, Solitons Fractals.*, vol. 155, p. 111715, 2022.

[29] D. Yan, M. Ji'e, L. Wang, et al, "Generating novel multi-scroll chaotic attractors via fractal transformation," *Nonlinear Dyn.*, vol. 107, no. 4, pp. 3919-3944, 2022.

[30] Q. Lai, Z. Wan, H. Zhang, et al, "Design and analysis of multiscroll memristive hopfield neural network with adjustable memductance and application to image encryption," *IEEE Trans. Neural Netw. Learn. Syst.*, DOI: 10.1109/TNNLS.2022.3146570, 2022.

[31] H. Lin, C. Wang, Y. Sun, et al, "Generating n-scroll chaotic attractors from a memristor-based magnetized Hopfield neural network," *IEEE Trans. Circuits Syst. II-Express Briefs.*, vol. 70, no. 1, pp. 311-315, 2023.

[32] M. Zand, M. A. Nasab, M. Khoobani, et al, "Robust speed control for induction motor drives using STSM control," *2021 12th Power Electronics, Drive Systems, and Technologies Conference (PEDSTC). IEEE.*, pp. 1-6, 2021.

[33] M. Khalili, M. Ali Dashtaki, M. A. Nasab, et al, "Optimal instantaneous prediction of voltage instability due to transient faults in power networks taking into account the dynamic effect of generators," *Cogent Eng.*, vol. 9, no. 1, p. 2072568, 2022.

[34] L. Chua, M. Komuro, T. Matsumoto. The double scroll family," *IEEE Trans. Circuits Syst.*, vol. 33, no. 11, pp. 1072-1118, 1986.

[35] H. Bao, Z. Hua, N. Wang, et al, "Initials-boosted coexisting chaos in a 2-D sine map and its hardware implementation," *IEEE Trans. Ind. Inform.*, vol. 17, no. 2, pp. 1132-1140, 2020.

[36] H. Lin, C. Wang, L. Cui, et al, "Brain-like initial-boosted hyperchaos and application in biomedical image encryption," *IEEE Trans. Ind. Inform.*, vol. 18, no. 12, pp. 8839-8850, 2022.

[37] E. N. Lorenz, "Deterministic nonperiodic flow," *Pac. J. Atmos. Sci.*, vol. 20, no. 2, pp. 130-141, 1963.

[38] S. M. Mohamed, W. S. Sayed, A. G. Radwan, et al, "FPGA implementation of reconfigurable CORDIC algorithm and a memristive chaotic system with transcendental nonlinearities," *IEEE Trans. Circuits Syst. I-Regul. Pap.*, vol. 69, no. 7, pp. 2885-2892, 2022.

[39] I. Koyuncu, A. T. Ozcerit, I. Pehlivan. "Implementation of FPGA-based real time novel chaotic oscillator," *Nonlinear Dyn.*, vol. 77, pp. 49-59, 2014.

[40] J. C. Sprott, "Some simple chaotic flows," *Phys. Rev. E.*, vol. 50, no. 2, pp. 647-650, 1994.

[41] G. Chen, T. Ueta, "Yet another chaotic attractor," *Int. J. Bifurcation Chaos.*, vol. 9, no. 07, pp. 1465-1466, 1999.

[42] N. T. Nguyen, T. Bui, G. Gagnon, et al, "Designing a pseudorandom bit generator with a novel five-dimensional-hyperchaotic system," *IEEE Trans. Ind. Electron.*, vol. 69, no. 6, pp. 6101-6110, 2021.

[43] M. A. Nasab, M. Zand, S. Padmanaban, et al, "An efficient, robust optimization model for the unit commitment considering renewable uncertainty and pumped-storage hydropower," *Comput. Electr. Eng.*, vol., 100, p. 107846, 2022.

[44] A. Rukhin, J. Soto, and J. Nechvatal, *A statistical test suite for random and pseudorandom number generators for cryptographic applications*, National Institute of Standards and Technology (NIST), Special Publication 800-22, Rev. 1a, Apr. 2010.

Hairong Lin (Member, IEEE) received M.S. and Ph.D. degree in information and communication engineering and computer science and technology from Hunan University, China, in 2015 and 2021, respectively. He is currently a postdoctoral research fellow at the College of Computer Science and Electronic Engineering, Hunan University, Changsha, China. He is an associate researcher at the Advanced Communication Technology Key Laboratory of Hunan University. He is a member of the Chaos and Nonlinear Circuit Professional Committee of Circuit and System Branch of China Electronic Society. He has presided over three national and provincial projects, and published more than 40 papers in related international journals, such as IEEE-TIE, IEEE-TII, IEEE-TCAD, IEEE-TCAS-I, IEEE-TCAS-II, Neural Networks, etc, among which 9 papers were highly cited and 3 papers were hot papers. His papers have been cited more than 1,200 times.

Dr. Lin is a Guest Editor of the journal of Mathematics from 2022 to present. He is also a Guest Editor of the journal of Frontiers in Physics from 2022 to present. Furthermore, he is a regular reviewer for many international journals, such as IEEE-TII, IEEE-TCAS-I, IEEE-TCAS-II, etc. His research interests include chaotic systems and circuits, memristors, memristive neural networks, medical image encryption, and neuromorphic engineering.
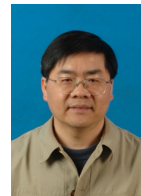
Chunhua Wang received the M.S. degree from Zhengzhou University, Zhengzhou, China, in 1994, and the Ph.D. degree from Beijing University of Technology, Beijing, China, in 2003. He is currently a Professor of College of Information Science and Engineering, Hunan University, Changsha, China. He is a Doctor tutor, the director of advanced communication technology key laboratory of Hunan universities, the member of academic committee of Hunan university, the director of chaos and nonlinear circuit professional committee of circuit and system branch of China electronic society. Now, his research interests include chaotic circuit, memristor circuit, chaotic encryption, neural networks based on memristor, complex network, current-mode circuit. He has presided over 8 national and provincial projects, and published more than 200 papers retrieved by SCI, among which 20 papers were high cited.

Prof. Wang was a recipient of Hunan Natural Science and Technology second prize in 2022. He was named to the Top 2% of Global Scientists in 2021 and 2022, and selected as the Highly Cited Researcher 2022 in Mathematics-field.

Yichuang Sun (M'90–SM'99) received the B.Sc. and M.Sc. degrees from Dalian Maritime University, Dalian, China, in 1982 and 1985, respectively, and the Ph.D. degree from the University of York, York, U.K., in 1996, all in communications and electronics engineering. Dr. Sun is currently Professor of Communications and Electronics, Head of Communications and Intelligent Systems Research Group, and Head of Electronic, Communication and Electrical Engineering Division in the School of Engineering and Computer Science of the University of Hertfordshire, UK. He has published over 330 papers and contributed 10 chapters in edited books. His research interests are in the areas of wireless and mobile communications, RF and analogue circuits, microelectronic devices and systems, and machine learning and deep learning.

Professor Sun was a Series Editor of IEE Circuits, Devices and Systems Book Series (2003-2008). He has been Associate Editor of IEEE Transactions on Circuits and Systems I: Regular Papers (2010-2011, 2016-2017, 2018-2019). He is also Editor of ETRI Journal, Journal of Semiconductors, and Journal of Sensor and Actuator Networks. He was Guest Editor of eight IEEE and IEE/IET journal special issues: High-frequency Integrated Analogue Filters in IEE Proc. Circuits, Devices and Systems (2000), RF Circuits and Systems for Wireless Communications in IEE Proc. Circuits, Devices and Systems (2002), Analogue and Mixed-Signal Test for Systems on Chip in IEE Proc. Circuits, Devices and Systems (2004), MIMO Wireless and Mobile Communications in IEE Proc. Communications (2006), Advanced Signal Processing for Wireless and Mobile Communications in IET Signal Processing (2009), Cooperative Wireless and Mobile Communications in IET Communications (2013), Software-Defined Radio Transceivers and Circuits for 5G Wireless Communications in IEEE Transactions on Circuits and Systems-II (2016), and the 2016 IEEE International Symposium on Circuits and Systems in IEEE Transactions on Circuits and Systems-I (2016). He has also been widely involved in various IEEE technical committee and international conference activities.